

Deceleration of C IV and Si IV broad absorption lines in X-ray bright quasar SDSS-J092345+512710

RAVI JOSHI,¹ RAGHUNATHAN SRINAND,² HUM CHAND,³ XUE-BING WU,^{1,4} PASQUIER NOTERDAEME,⁵ PATRICK PETITJEAN,⁵
AND LUIS C. HO^{1,4}

¹*Kavli Institute for Astronomy and Astrophysics, Peking University, Beijing 100871, China*

²*Inter-University Centre for Astronomy and Astrophysics, Post Bag 4, Ganeshkhind, Pune 411007, India*

³*Aryabhata Research Institute of Observational Sciences (ARIES), Manora Peak, Nainital – 263 002, India*

⁴*Department of Astronomy, School of Physics, Peking University, Beijing 100871, China*

⁵*Institut d’Astrophysique de Paris, UMR 7095, CNRS-SU, 98bis bd Arago, 75014 Paris, France*

ABSTRACT

We report a synchronized kinematic shift of C IV and Si IV broad absorption lines (BAL) in a high-ionization, radio-loud, and X-ray bright quasar SDSS-J092345+512710 (at $z_{\text{em}} \sim 2.1627$). This quasar shows two broad absorption components (blue component at $v \sim 14,000 \text{ km s}^{-1}$, and red component at $v \sim 4,000 \text{ km s}^{-1}$ with respect to the quasars systemic redshift). The absorption profiles of C IV and Si IV BAL of the blue component show decrease in outflow velocity with an average deceleration rate of $-1.62^{+0.04}_{-0.05} \text{ cm s}^{-2}$ and $-1.14^{+0.21}_{-0.22} \text{ cm s}^{-2}$ over a rest-frame time-span of 4.15 yr. We do not see any acceleration signature in the red component. This is consistent with dramatic variabilities usually seen at high velocities. During our monitoring period the quasar has shown no strong continuum variability. We suggest the observed variability could be related to the time dependent changes in disk wind parameters like launching radius, initial flow velocity or mass outflow rate.

Keywords: galaxies: active - quasars: absorption lines - quasars: general quasars: individual: J092345+512710.

1. INTRODUCTION

Outflows are ubiquitous and appear to be the main agent of active galactic nucleus (AGN) feedback which regulates black hole growth and host galaxy evolution as well as enrich the intergalactic and circumgalactic medium around galaxies (see Ostriker et al. 2010; Komremdy & Ho 2013). These feedback processes most likely drive the well-known observed correlation between the supermassive black hole (SMBH) mass and physical properties of the host galaxy, along with the steep decline of the number density of galaxies at high masses (Ferrarese & Merritt 2000; Hopkins et al. 2005; Ostriker et al. 2010). The signature of strong outflows are directly observed in roughly 20 percent of quasar population via broad ultraviolet-resonance absorption lines (BAL) (Weymann et al. 1991; Trump et al. 2006; Gibson et al. 2009), spanning a large range of outflow velocities from 1000 km s^{-1} up to several $10,000 \text{ km s}^{-1}$ (e.g., Weymann et al. 1991; Hamann et al. 1997; Rodríguez

Hidalgo et al. 2011; Rogerson et al. 2016). Nonetheless, many aspects of quasar outflows remain poorly understood, including the gas geometry, acceleration mechanism(s) and their influence on the host galaxy and its environments.

BAL variability study is a promising technique for constraining the structure and locations of the associated wind. In recent systematic studies of BAL variability, BAL troughs are commonly observed to vary in absorption strength (Barlow 1994; Lundgren et al. 2007; Gibson et al. 2008; Capellupo et al. 2011, 2012, 2013; Filiz Ak et al. 2013; Vivek et al. 2014; Grier et al. 2015; McGraw et al. 2018) and/or profile, also known as “transient BALs” showing emergence or disappearance of BAL features (e.g., Hamann et al. 2008; Hall et al. 2011; Rodríguez Hidalgo et al. 2011; Filiz Ak et al. 2012; Vivek et al. 2016; McGraw et al. 2017), over a broad range of rest-frame timescales, ranging from months to years. However, the signature of acceleration (e.g., kinematic shift of absorption profile) are more scarce, reported only a few times (e.g., Vilkoviskij & Irwin 2001; Rupke et al. 2002; Gabel et al. 2003; Hall et al. 2007; Joshi et al. 2014; Grier et al. 2016). Mechanisms pro-

posed to understand the observed BAL variability are supposed to be changes in ionization state and/or the movement of individual clouds or substructures in the outflow, across our line of sight (Lundgren et al. 2007; Hall et al. 2007; Hamann et al. 2008). In most cases the BAL variations are not found to be correlated with the optical continuum variations. Also not all velocity components seen in absorption show correlated variations. This hints towards mechanisms other than photoionization induced variations. However, a unified understanding of BAL variations is an ongoing endeavor.

The BAL features are widely believed to be formed in “disk winds”, launched from the surface of the accretion disk at 10-100 light days from the central SMBH (of $\sim 10^9 M_{\odot}$) mainly driven by radiative forces (Arav & Li 1994; Murray et al. 1995; Proga 2000; Higginbottom et al. 2014). In radiation-driven scenarios, the wind is efficiently accelerated to high velocities by invoking the shielding gas close to the base of outflow which prevent the UV-absorbing gas from becoming overionized by nuclear X-ray and extreme-ultraviolet(UV) photons (Murray et al. 1995; Proga 2000). The above paradigm is challenged by the observed flows having high velocities and lower degree of ionization in X-ray bright mini-BAL (typical full width half maximum of $500 - 2000 \text{ km s}^{-1}$) quasars (Hamann et al. 2008, 2013). These observations favor the substructured flow, involving tiny dense clouds with a low volume filling factor, driven out by radiative forces while being confined by magnetic pressure (Rees 1987; Baskin et al. 2014; Matthews et al. 2016). It suggests that the strong radiative shielding gas may not be universal component of quasar outflows for accelerating the gas to high speeds. This idea is also supported by the recent high-energy X-ray observations showing that a large fraction, $\sim 6 - 23\%$, of BAL quasars among the general BAL quasar population are perhaps intrinsically X-ray weak in nature (Luo et al. 2013, 2014; Teng et al. 2014; Liu et al. 2018).

The emerging picture of BAL outflows suggests that the mini-BALs and BALs arise from the same quasar wind, where BALs form in the main part of the outflow near the accretion disc plane while mini-BALs form along sightlines at higher latitudes (Ganguly et al. 2001; Hamann et al. 2008, 2013). This also explains the observed X-ray bright nature of mini-BALs. Interestingly, a new population of X-ray bright BAL quasars is recently discovered in X-ray surveys (e.g., Giustini et al. 2008; Gibson et al. 2009; Streblyanska et al. 2010; Liu et al. 2018) which further possess major challenges to the models of BAL outflows. Note that, if the X-ray bright BAL quasars are preferentially originated in a structured flow viewed along the sight lines of higher

latitudes than one would naively expect to see the combination of line shift and line strength variability in this subclass. Indeed, in our recent efforts to probe the variability nature of X-ray bright BAL quasars we have find two such rare cases of kinematic shift and strength variability of the C IV BAL trough (e.g., Joshi et al. 2014). Given the X-ray weak nature of general population of BAL quasars, a systematic study of this rare population of X-ray bright BAL quasars will provide important observational constrains on the BAL geometry and the physical mechanisms for launching and accelerating the quasar outflows.

Here, we report the detection of a decelerating C IV and Si IV BAL outflow towards X-ray bright quasar J092345+512710. This source is part of our on going monitoring program of BAL spectral variability in rare X-ray bright BAL quasars (see, Joshi et al. 2014). This paper is organized as follows. Section 2 describes the observations and data reduction. In Section 3, we present the results of our analysis followed with the discussion and conclusion in Section 4.

2. OBSERVATION AND DATA REDUCTION

The BAL quasar J092345+512710 was first detected in Sloan Digital Sky Survey (Trump et al. 2006) which we have followed with 2-metre telescope at IUCAA Girawali Observatory (IGO), using IUCAA Faint Object Spectrograph and Camera (IFOSC). We performed a long-slit spectroscopic observation of this target on 2011 April 1. In order to cover the C IV and Si IV BAL troughs we have used Grism¹ #7 of IFOSC, in combination with a 1.5 arcsec slit. This yielded a wavelength coverage of 3800–6840 Å at a spectral resolution $R \sim 1140$ (i.e., $\sim 310 \text{ km s}^{-1}$). We acquired 2 exposures of 45 minutes each. The raw CCD frames were cleaned using standard IRAF² procedures. We carried out the bias and flat-field corrections to all the frames. The Halogen flats were used for flat fielding the frames. We then extracted the one-dimensional spectrum from individual frames using the IRAF task “apall”. Wavelength calibration was done using the standard Helium-Neon lamp spectra and flux calibration was done using standard star observed on the same night. We applied air-to-vacuum conversion and coadded the spectra, using $1/\sigma_i^2$ weighting in each pixel, after scaling the overall individual spectrum to a common flux level. Subsequently the quasar was observed

¹ <http://www.iucaa.ernet.in/~itp/etc/ETC/help.html#grism>

² IRAF is distributed by the NATIONAL OPTICAL ASTRONOMY OBSERVATORIES, which are operated by the Association of Universities for Research in Astronomy, Inc., under cooperative agreement with the National Science Foundation.

twice again as part of SDSS-BOSS survey. This four epochs data forms the major resource for the analysis presented here. Details are given in Table 1.

We also used photometric light curves from publicly available Catalina Real-Time Transient Survey³ (CRTS) to judge the amount of flux variations seen in this quasar.

2.1. Continuum Fitting

Following Gibson et al. (2009), we model the quasar continuum emission using a Small Magellanic Cloud-like reddened power-law function from Pei (1992). We use the emission redshift of $z_{\text{em}} = 2.16274$, from Hewett & Wild (2010) to get the rest frame quasar spectrum and fit only regions largely free from emission and absorption features which are in ranges 1280 – 1300 Å, 1700 – 1800 Å, 1950 – 2200 Å, 2650 – 2710 Å, and 2950 – 3700 Å. To the uncertainties over the continuum fit, we performed Monte Carlo simulations by randomizing the flux in each pixel with a random Gaussian deviate associated with uncertainty over the pixel. We fit the continuum to the new spectrum over 100 times and adopt their standard deviation as the uncertainties of the continuum fit.

In addition, to remove the emission line features we model them using Gaussian profiles over continuum subtracted spectra, without associating any physical meaning. Note that, modelling the C IV emission is nontrivial as the line profile is usually asymmetric and blanket with multiple strong absorption features. Therefore, to model the C IV emission profile we exclude the wavelength ranges having absorption signature and fit the remaining C IV feature using a double Gaussian profile. We model the Si IV emission line with a single Gaussian. The final continuum fit (solid line), comprising of a power law for the line free continuum and the multi-Gaussian components for the broad emission lines is shown in top panel of Fig. 1. The flux uncertainties from both the continuum fit and flux measurement errors were propagated to determine the final uncertainty on the normalized spectrum. Finally, we generate the continuum-normalized spectra to examine the BAL variability.

3. ANALYSIS

J092345+512710 is a HiBAL quasar having smooth C IV and Si IV BAL profiles at a similar outflow velocity of $v \sim -9000$ to $-20,000$ km s⁻¹ (see, top panel of Fig. 1). We refer to this as “blue” component (marked as

‘B’ in Fig 1). We also detect N v absorption corresponding to that of C IV BAL trough in the BOSS spectra of Epoch 3 and 4 at very blue part of the spectra having poor S/N. There is a hint of weak Ly α absorption at a similar velocity as the C IV BAL. In addition, we also detect associated C IV and N v absorption component with $v \sim -1000$ to -6000 km s⁻¹ composed of several narrow components. We refer to this as “red” component (marked as ‘R’ in Fig 1). The Si IV is found to be weak in this component. We also searched for the additional BAL features in the spectrum but there are no Al III and Mg II BALs at the corresponding position of C IV BAL trough.

In Figure 1, lower sub-panels, we compare the continuum normalized C IV and Si IV absorption line profiles (smoothed over 3 pixels) in IGO spectrum MJD-55652 (Epoch 2) and SDSS spectrum from epoch MJD-52252 (Epoch 1), MJD-56607 (Epoch 3) with a reference BOSS spectrum obtained in MJD-57046 (i.e., year 2015), in velocity scale with $v = 0$ km s⁻¹ corresponding to systemic redshift of the quasar, i.e., $z_{\text{em}} = 2.1627$. A decrease in radial velocity for both C IV and Si IV BAL troughs in the “blue” component is apparent in high signal-to-noise (S/N) ratio spectra between Epochs 1 and 4, over a rest frame time scale of 4.15 years. Interestingly, a clear signature of velocity shift for the C IV component is also seen in our low S/N IGO spectrum (see, left sub panels of Fig. 1), over a rest-frame time span of 2.95 years and 1.21 years between Epoch 1 and 2 and Epoch 2 and 4, respectively. However, no such kinematic shift is seen between Epoch 3 and 4 over relatively shorter rest frame time span of ~ 0.38 years. Additionally, for the “red” component that shows sub-components we do not find any kinematic shift which ensures that the observed kinematic shift in the “blue” BAL trough is real. We note that our IGO (Epoch 2) spectrum is too noisy at shorter wavelengths where Si IV absorption is present, hence, we do not use it further to study the Si IV BAL variability. Unfortunately, as the N v region is not covered in the early epoch SDSS and IGO spectrum that prevents us from studying the kinematic shift of N v.

To quantify the kinematic shift of BAL trough, specifically blue component, between two epochs spectra we perform a cross-correlation function (CCF) analysis (see also, Grier et al. 2016). For this, we consider the spectral region including the BAL trough in question plus 2000 km s⁻¹ on each side and measure the cross-correlation coefficient (τ) by shifting the early epoch spectrum with 1 pixel step (i.e., 69 km s⁻¹) over a velocity range of -6000 to $+6000$ km s⁻¹. We measure the velocity shift as the most significant peak of correlation coefficient and the centroid of CCF using only points around the peak

Table 1. Information related to observations and other basic parameters of J092345+512710 spectra and its BAL trough.

Instrument	Date (Epoch,yy.mm.dd) (MJD)	Exposure Time (mins)	Resolution (km s ⁻¹)	S/N ^a	W_{1549} ^b (Å)	W_{1400} (Å)	W_{1549}/W_{1400}
SDSS	52252 (#1, 2001.09.12)	80×1	150	11	14.0 ± 0.5	9.4 ± 0.5	1.5±0.1
IGO/IFOSC 7 ^c	55652 (#2, 2011.07.01)	45×2	310	4	17.7 ± 1.3	11.8 ± 1.1	1.5±0.2
SDSS-BOSS	56607 (#3, 2013.11.11)	75×1	150	14	20.8 ± 0.3	8.8 ± 0.3	2.5±0.1
SDSS-BOSS	57046 (#4, 2015.24.01)	90×1	150	11	19.1 ± 0.4	6.1 ± 0.4	3.1±0.2

^a Signal-to-noise ratio per-pixel over the wavelength range 5100–5500 Å.

^b W_{1549} is measured over a velocity range of -22,576 to -8,735 km s⁻¹.

^c Wavelength Coverage of 3800–6840 Å.

(i.e, with $\tau > 0.8 r_{\text{peak}}$). In order to account for the measurement uncertainties we perform the Monte Carlo simulations, randomizing the fluxes of both spectra by a random Gaussian deviate associated with uncertainty over each pixel. We generate 1000 such realizations and measure the CCF and the corresponding peak and centroid for each realization of spectra. We take the median of the cross correlation centroid distribution (CCCD) as final velocity shift and 1σ uncertainty as the central interval encompassing 68% of CCCD. The measured CCF and cross correlation centroid distribution for two spectra from Epoch 1 and 4 are shown in lower-left and lower-right panels of Fig. 2. The best velocity shift and the corresponding deceleration values between different epochs for C IV and Si IV components are given in columns 4, 5 and 8, 9 of Table 2, respectively.

The average deceleration for “blue” C IV BAL component is found to be $-1.62_{-0.05}^{+0.04}$ cm s⁻² between Epochs 1 and 4, over a rest frame time scale of 4.15 years. However, the average measured deceleration may not be constant over time. We measure a deceleration of magnitude $-1.18_{-0.16}^{+0.17}$ cm s⁻² between Epochs 1 and 2 which increase to $-1.61_{-0.25}^{+0.30}$ cm s⁻², only at $\sim 1.3 \sigma$ level, between Epochs 2 and 4. A similar average deceleration is also observed for the Si IV BAL component (see column 9 of Table 2). We have also given the upper limits for the cases where no significant acceleration is detected. It is worth noting that based on very few cases of BAL kinematic shift reported in the literature (Gabel et al. 2003; Grier et al. 2016) the wind acceleration is not found to be constant when multiple epochs are compared.

Next, we test the variability in strength and/or shape of BAL profile as the highly variable optical depths may also mimic the actual deceleration (specific to our case) signatures. For this, we perform a χ^2 test between different epoch spectra by applying a measured velocity shift to the later epoch spectrum (see, top panel of Fig 2). The reduced χ^2_{ν} and corresponding null probability p of BAL profile being similar between two epochs for

C IV and Si IV BAL components are listed in column 6, 7 and 10, 11 of Table 2, respectively. The higher value of p would imply that the C IV BAL profile is similar between Epoch 1 vis-a-vis 2 and Epoch 2 vis-a-vis 3 but show a significant variability between Epoch 1 and 3 and Epoch 1 and 4. Similarly, the probability of Si IV BAL profile to be different between Epoch 1 and 3 is less than 10%, whereas, shows a significant difference between epoch 1 and 4 (see also, Table 2). A similar trend can also be seen from the measured rest frame C IV (W_{1549}) and Si IV (W_{1400}) equivalent width between different epochs, listed in column 6 and 7 of Table 1. The change in W_{1549} between Epoch 1 to 2 and Epoch 2 to 3 is significant at only 2.7σ and 2.3σ level, respectively. For Si IV BAL, the difference in W_{1400} between Epoch 1 and 3 is marginal (at 1.0σ) but between Epoch 1 and 4 is significant at 5.5σ level. Note that, both C IV and Si IV absorption do shows saturation which either imply an optically thin absorption or partial coverage. Since, Si IV optical depth is smaller than C IV and both absorption are well detached from the corresponding emission it indicates that Si IV is optically thin even if C IV is saturated. While the overall profile shape has not changed, however, the equivalent width ratio of Si IV/C IV has changed by up to a factor of two (see, column 8 of Table 1). Since, C IV may be saturated, as a result its profile variation will be minimal compare to the Si IV when there is any change in ionizing condition (either due to quasar luminosity change or cloud density or change in the distance between the absorbing gas and quasar). It is also clearly evident from Fig. 1 that overall shape of the absorption profile of the C IV and Si IV BALs is quite similar over all the epochs, except a moderate broadening of C IV BAL in Epoch 3 and 4. CRTS V -mag light curve is available between MJD 53700 and 56545, which does not show any systematic brightening/dimming of the source though short time-scale fluctuations may be present. The mean V mag is 19.22 with a σ of 0.49 mag. Thus the long time-scale

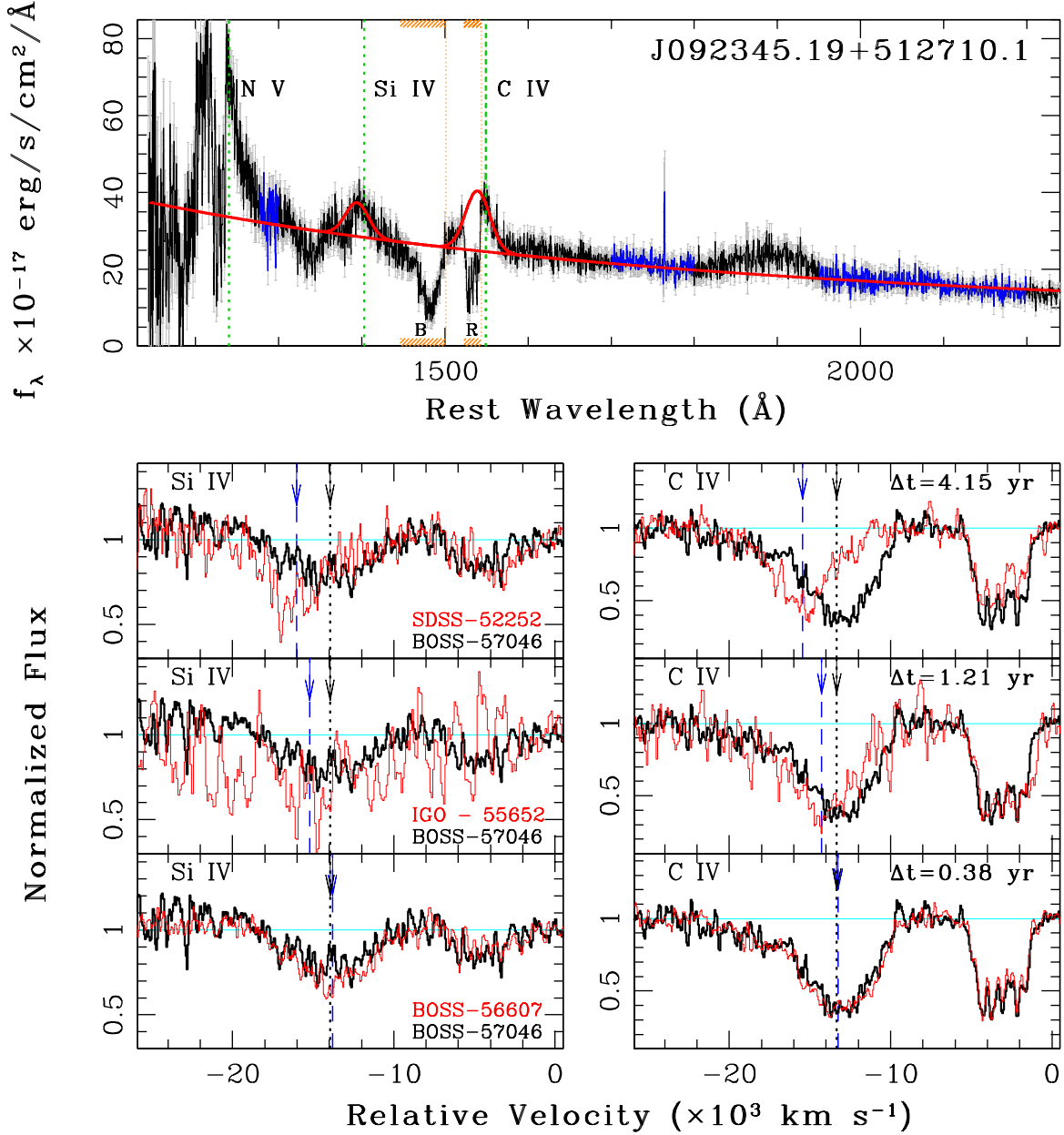


Figure 1. Upper panel: The final continuum fit (smooth curve) comprising of a power law and the multiple-Gaussian components for BOSS MJD-57046 (Epoch 4) spectrum. The hatched region show the “blue” and “red” C IV absorption profiles and marked as ‘B’ and ‘R’, respectively. The blue data intervals represent the relatively line-free windows chosen for the power-law fit. Lower Panel: The comparison of continuum-normalized C IV (right sub panels) and Si IV (left sub panels) absorption line profiles (smoothed over 3 pixels) in SDSS MJD-52252 (Epoch 1), IGO MJD-55652 (Epoch 2), and BOSS MJD-56607 (Epoch 3) spectrum (red, thin solid line) with reference BOSS MJD-57046 (Epoch 4) spectrum (black, thick solid line). The velocity scale, with $v = 0 \text{ km s}^{-1}$ corresponding to quasar emission redshift of $z_{\text{em}} = 2.1627$. The velocity centroid of absorption trough for reference (Epoch 4) and comparison spectrum are shown with arrow and also with dotted and dashed lines, respectively.

equivalent width variations may not be linked to quasar flux variation.

The main point to understand now is the deceleration signature shown by the “blue” component with very

similar profile at different epochs albeit having mild evolution in the observed rest equivalent widths. Below we consider different possibilities.

Table 2. Kinematic shift measurements for C IV and Si IV BALs in J092345+512710.

Spectra		Δt^a (years)	C IV BAL				Si IV BAL					
			Vel shift (km s ⁻¹)	Accel (cm s ⁻²)	Shifted		Vel shift (km s ⁻¹)	Accel (cm s ⁻²)	Shifted			
(1)	(2)	(3)	(4)	(5)	χ^2_ν	p	(6)	(7)	(8)	(9)	χ^2_ν	p
SDSS-52252	IGO-55652	2.95	-1098^{+158}_{-151}	$-1.18^{+0.17}_{-0.16}$	0.74	0.99	—	—	—	—	—	—
IGO-55652	BOSS-57046	1.21	-613^{+114}_{-95}	$-1.61^{+0.30}_{-0.25}$	0.83	0.94	—	—	—	—	—	—
SDSS-52252	BOSS-56607	3.77	-2072^{+62}_{-63}	$-1.74^{+0.05}_{-0.05}$	2.20	0.00	-1855^{+272}_{-167}	$-1.56^{+0.23}_{-0.14}$	1.16	0.10		
SDSS-52252	BOSS-57046	4.15	-2126^{+59}_{-66}	$-1.62^{+0.04}_{-0.05}$	1.66	0.00	-1491^{+280}_{-290}	$-1.14^{+0.21}_{-0.22}$	1.29	0.01		
BOSS-56607	BOSS-57046	0.38	55^{+32}_{-33}	< 0.96	1.26	0.01	99^{+126}_{-69}	< 2.07	1.17	0.10		

^a time-scale measured in the quasar rest frame

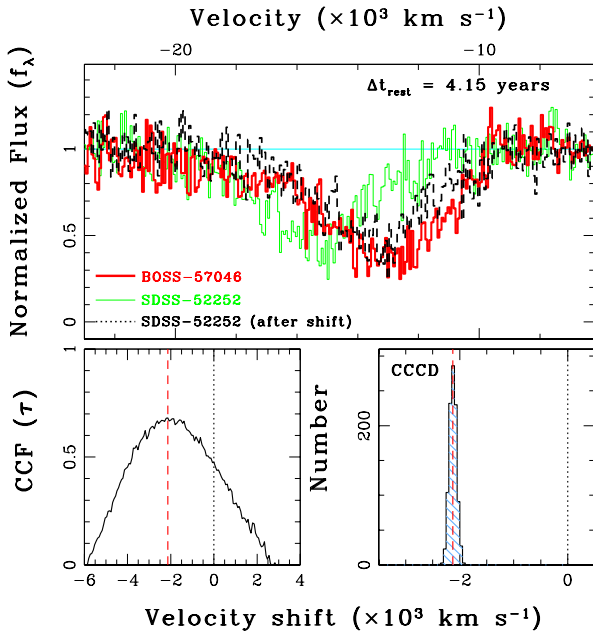


Figure 2. Top Panel: The comparison of C IV BAL profile between SDSS (Epoch 1) and BOSS (Epoch 4) spectra. The SDSS spectrum before and after shifting by the measured velocity shift from CCF analysis is shown in thin solid line (green) and dotted line, respectively. Bottom Panel: The cross-correlation function (CCF) for the Epoch 1 and 4 spectra and cross correlation centroid (CCCD) distribution from Monte-Carlo simulations are given in bottom-left and bottom-right panels, respectively. The centroid shift of BAL profile is given in dashed line with zero velocity point in dotted line.

4. DISCUSSION AND CONCLUSIONS

We report on the kinematic shift of C IV and Si IV BAL profiles in a radio-loud quasar SDSS-J092345+512710. It belongs to a rare sub-class of X-ray bright BAL quasar with a neutral hydrogen column density of $N_{\text{H}} < 3 \times 10^{22} \text{ cm}^{-2}$ and an optical to X-ray spectral index, α_{ox} , of ~ -1.59 which is greater than the typical α_{ox} mea-

sured for soft X-ray weak quasars, i.e., $\alpha_{ox} < -2$ (Giustini et al. 2008). In addition, the difference between observed α_{ox} and expected α_{ox} from the UV luminosity, i.e., $\Delta\alpha_{ox}$, is found to be 0.04 (Giustini et al. 2008). We detect an average acceleration of $-1.62 \pm 0.04 \text{ cm s}^{-2}$ and $-1.14 \pm 0.21 \text{ cm s}^{-2}$ in C IV and Si IV BALs trough, respectively, over a rest-frame time span of 4.15 years (Table 2). We do not find any acceleration signature for the “red” component. Interestingly, we find that the measured deceleration for “blue” C IV BAL may not be constant over time, the rate of deceleration between Epoch 2 and 4 is more rapid, about factor 1.4 (significant at only 1.3σ level) higher than Epoch 1 and 2.

In the handful of previous studies of the kinematic shift in individual objects Vilkoviskij & Irwin (2001), Rupke et al. (2002) and Hall et al. (2007) have measured a positive kinematic shift (i.e., acceleration) of BAL with a typical acceleration rate of $0.035 \pm 0.016 \text{ cm s}^{-2}$, $0.08 \pm 0.03 \text{ cm s}^{-2}$, and $\sim 0.0154 \pm 0.025 \text{ cm s}^{-2}$ respectively. The first detection of negative kinematic shift (i.e., deceleration) is reported by Gabel et al. (2003) in the Seyfert galaxy NGC 3783. Using the multi-epoch observations they have found a synchronous kinematic shift of C IV, Si IV, N V absorption features, while preserving the absorption profile, with a varying deceleration rate which raises from $-0.1 \pm 0.03 \text{ cm s}^{-2}$ to $-0.25 \pm 0.05 \text{ cm s}^{-2}$ in the later interval. In addition, Joshi et al. (2014) have detected relatively larger deceleration rate of $-0.7 \pm 0.1 \text{ cm s}^{-2}$ and $-2.0 \pm 0.1 \text{ cm s}^{-2}$ of C IV BAL in two X-ray bright BAL quasars over rest-frame time-spans of 3.11 and 2.34 yr. Recently, Grier et al. (2016) have performed the first systematic search for BAL acceleration using three epoch SDSS spectra of 140 BAL quasars over timescales of 2.5–5.5 years and found only 3 cases, two acceleration and one deceleration, of monolithic velocity shift showing an overall lack of widespread BAL acceleration. They have measured an average acceleration/deceleration rate of $0.63^{+0.14}_{-0.13} \text{ cm s}^{-2}$, $0.54 \pm 0.04 \text{ cm s}^{-2}$ and $-0.83^{+0.19}_{-0.24} \text{ cm s}^{-2}$

s^{-2} , which is comparable to the present study. Using the upper limits for C IV BAL acceleration and deceleration in 76 BAL troughs, over a rest-frame timescales of 2.5 to 5.5 years, they show that the majority of BALs exhibit stable mean velocities to within about 3 per cent. Interestingly, for all the three cases they have found that the wind acceleration rate is not constant over the time.

The observed kinematic shift in BAL can be produced due to several reasons e.g., actual line-of-sight acceleration of a shell of material from an intermittent outflow, directional shift in the outflow, and changes in velocity dependent quantities such as ionization state, or covering factor (Hall et al. 2002; Gabel et al. 2003; Hall et al. 2007). At first, we consider the simplest case of changing radiation energy which will lead to decrease in the injected momentum and thus will slow down the wind. As mentioned before using the CRTS light curve we find that our source shows a negligible variation, less than order of half a magnitude, over the time spanned by our observations. In addition, we do not see any significant variation in the emission line flux which responds to the continuum. So we conclude that change in radiative energy/momentum may not be the primary source of deceleration.

Secondly, we consider the possibility of gravitational force for the bulk radial deceleration of the flow. Most of the accretion disk wind models predicts the BAL outflow at a typical distance of 0.01 pc from the central source (Murray et al. 1995; Proga 2000) whereas the observations suggest that the outflows are located at much larger distances in the range of parsecs to several kilo-parsecs. Recently, using Si IV BAL trough Xu et al. (2018) have shown that about more than 75% of BAL outflows are at > 100 pc (see also, Arav et al. 2018, and references therein). Given the central black hole mass of J092345+512710 to be $3 \times 10^9 M_{\odot}$ (Shen et al. 2011) and assuming the absorbing cloud is at a typical distance of 1 pc from the central ionizing source where gravity is mainly dominated by the black hole, at the SDSS Epoch 1 we find that the escape velocity is much lower ($\sim 5081 \text{ km s}^{-1}$) than the average outflow speed of $15,000 \text{ km s}^{-1}$. It indicates that the observed deceleration of the outflow is very unlikely caused by the deceleration of continual flow due to gravitational force. Alternatively, if we consider the absorbing clouds to be at larger distances, it is quite plausible that the outflowing gas may interact with the ambient material in the host galaxy which in turn may cause the deceleration of BAL winds (see, Leighly et al. 2014). In such scenario the interaction will also change the ionization and thermal state of the gas thereby introducing profile variation. This is not evident from the observed BAL

profiles. In view of the fact that majority of BALs are stable within 3 percent of their mean velocity Grier et al. (2016) argue that BAL cloud may not have traveled sufficiently far to interact with the ambient medium. However, more such examples of BAL deceleration will be crucial to test this scenario.

In disk wind models the BAL profiles are produced by a steady wind whose density and velocity as a function of radius is governed by force equation (balance between radiative acceleration and gravity) and mass and momentum conservation at all radial distances ' r '. It is also known that parameters such as the initial injection position and velocity of the wind and mass outflow rate will alter velocity and density at a radial distance from quasar (for example, see the basic set of equations given in Section 2.4.2 of Borguet & Hutsemékers 2010). Therefore, even if the quasar luminosity does not change any time variation in the initial condition of the wind (launch radius, initial velocity, and mass outflow rate) can lead to acceleration or deceleration signatures (see Section 4.1 of Grier et al. 2016).

It may be noted that, absorption profile change introduced by the radial velocity profile change and associated density profile change due to continuity equation will also produce ionization change effects (even when radiation field remains constant). Therefore, while producing velocity shift one will have independent constraints from the equivalent width and equivalent width ratio variations. However, one may have to exercise caution as equivalent width variations without apparent profile shape variations could just be caused by variations in the covering factor. A detailed study on this issue is interesting and important for our understanding of BAL flows. Also, high signal to noise spectra at higher spectral resolution will be important to further constrain the outflow models.

In our BAL variability studies of X-ray bright BALQSOs till now we have found significant profile shift in three cases. Joshi et al. (2014) reported two cases of deceleration. Unlike in the present case the deceleration is also accompanied by profile shape variation in other two cases. However, there are few common trends we notice in all three cases: (i) The decelerating components typically have large ejection velocities (i.e., $> 10,000 \text{ km s}^{-1}$); (ii) There is associate absorption at low velocities without showing any signatures of acceleration; and (iii) the optical quasar continuum has not varied appreciably. Additionally, it is intriguing that we have not yet seen acceleration signatures in X-ray BALs combined to the fact of high frequency of occurrence of deceleration in them compared to the X-ray weak typical BALs. Confirmation of this trend in large sample will be interesting

for understanding the physical origin of X-ray loudness (or weakness) of BAL quasars.

ACKNOWLEDGMENTS

This work was supported by the National Key R&D Program of China (2016YFA0400702, 2016YFA0400703) and the National Science Foundation of China (11473002, 11721303, 11533001).

Funding for the Sloan Digital Sky Survey IV has been provided by the Alfred P. Sloan Foundation, the U.S. Department of Energy Office of Science, and the Participating Institutions. SDSS-IV acknowledges support and resources from the Center for High-Performance Computing at the University of Utah. The SDSS web site is www.sdss.org.

SDSS-IV is managed by the Astrophysical Research Consortium for the Participating Institutions of the SDSS Collaboration including the Brazilian Participation Group, the Carnegie Institution for Science, Carnegie Mellon University, the Chilean Participa-

tion Group, the French Participation Group, Harvard-Smithsonian Center for Astrophysics, Instituto de Astrofísica de Canarias, The Johns Hopkins University, Kavli Institute for the Physics and Mathematics of the Universe (IPMU) / University of Tokyo, Lawrence Berkeley National Laboratory, Leibniz Institut für Astrophysik Potsdam (AIP), Max-Planck-Institut für Astronomie (MPIA Heidelberg), Max-Planck-Institut für Astrophysik (MPA Garching), Max-Planck-Institut für Extraterrestrische Physik (MPE), National Astronomical Observatories of China, New Mexico State University, New York University, University of Notre Dame, Observatório Nacional / MCTI, The Ohio State University, Pennsylvania State University, Shanghai Astronomical Observatory, United Kingdom Participation Group, Universidad Nacional Autónoma de México, University of Arizona, University of Colorado Boulder, University of Oxford, University of Portsmouth, University of Utah, University of Virginia, University of Washington, University of Wisconsin, Vanderbilt University, and Yale University.

REFERENCES

- Arav, N., & Li, Z.-Y. 1994, *ApJ*, 427, 700
 Arav, N., Liu, G., Xu, X., et al. 2018, *ApJ*, 857, 60
 Barlow, T. A. 1994, *PASP*, 106, 548
 Baskin, A., Laor, A., & Stern, J. 2014, *MNRAS*, 445, 3025
 Borguet, B., & Hutsemekers, D. 2010, *A&A*, 515, A22
 Capellupo, D. M., Hamann, F., Shields, J. C., Halpern, J. P., & Barlow, T. A. 2013, *MNRAS*, 429, 1872
 Capellupo, D. M., Hamann, F., Shields, J. C., Rodríguez Hidalgo, P., & Barlow, T. A. 2011, *MNRAS*, 413, 908
 —. 2012, *MNRAS*, 422, 3249
 Ferrarese, L., & Merritt, D. 2000, *ApJ*, 539, L9
 Filiz Ak, N., Brandt, W. N., Hall, P. B., et al. 2012, *ApJ*, 757, 114
 —. 2013, *ApJ*, 777, 168
 Gabel, J. R., Crenshaw, D. M., Kraemer, S. B., et al. 2003, *ApJ*, 595, 120
 Ganguly, R., Bond, N. A., Charlton, J. C., et al. 2001, *ApJ*, 549, 133
 Gibson, R. R., Brandt, W. N., & Schneider, D. P. 2008, *ApJ*, 685, 773
 Gibson, R. R., Jiang, L., Brandt, W. N., et al. 2009, *ApJ*, 692, 758
 Giustini, M., Cappi, M., & Vignali, C. 2008, *A&A*, 491, 425
 Grier, C. J., Hall, P. B., Brandt, W. N., et al. 2015, *ApJ*, 806, 111
 Grier, C. J., Brandt, W. N., Hall, P. B., et al. 2016, *ApJ*, 824, 130
 Hall, P. B., Anosov, K., White, R. L., et al. 2011, *MNRAS*, 411, 2653
 Hall, P. B., Sadavoy, S. I., Hutsemekers, D., Everett, J. E., & Rafiee, A. 2007, *ApJ*, 665, 174
 Hall, P. B., Anderson, S. F., Strauss, M. A., et al. 2002, *ApJS*, 141, 267
 Hamann, F., Barlow, T. A., & Junkkarinen, V. 1997, *ApJ*, 478, 87
 Hamann, F., Chartas, G., McGraw, S., et al. 2013, *MNRAS*, 435, 133
 Hamann, F., Kaplan, K. F., Rodríguez Hidalgo, P., Prochaska, J. X., & Herbert-Fort, S. 2008, *MNRAS*, 391, L39
 Hewett, P. C., & Wild, V. 2010, *MNRAS*, 405, 2302
 Higginbottom, N., Proga, D., Knigge, C., et al. 2014, *ApJ*, 789, 19
 Hopkins, P. F., Hernquist, L., Cox, T. J., et al. 2005, *ApJ*, 630, 705
 Joshi, R., Chand, H., Srianand, R., & Majumdar, J. 2014, *MNRAS*, 442, 862
 Kormendy, J., & Ho, L. C. 2013, *ARA&A*, 51, 511
 Leighly, K. M., Terndrup, D. M., Baron, E., et al. 2014, *ApJ*, 788, 123
 Liu, H., Luo, B., Brandt, W. N., Gallagher, S. C., & Garmire, G. P. 2018, *ArXiv e-prints*, arXiv:1804.05074
 Lundgren, B. F., Wilhite, B. C., Brunner, R. J., et al. 2007, *ApJ*, 656, 73

- Luo, B., Brandt, W. N., Alexander, D. M., et al. 2013, *ApJ*, 772, 153
- . 2014, *ApJ*, 794, 70
- Matthews, J. H., Knigge, C., Long, K. S., et al. 2016, *MNRAS*, 458, 293
- McGraw, S. M., Shields, J. C., Hamann, F. W., Capellupo, D. M., & Herbst, H. 2018, *MNRAS*, 475, 585
- McGraw, S. M., Brandt, W. N., Grier, C. J., et al. 2017, *MNRAS*, 469, 3163
- Murray, N., Chiang, J., Grossman, S. A., & Voit, G. M. 1995, *ApJ*, 451, 498
- Ostriker, J. P., Choi, E., Ciotti, L., Novak, G. S., & Proga, D. 2010, *ApJ*, 722, 642
- Pei, Y. C. 1992, *ApJ*, 395, 130
- Proga, D. 2000, *ApJ*, 538, 684
- Rees, M. J. 1987, *QJRAS*, 28, 197
- Rodríguez Hidalgo, P., Hamann, F., & Hall, P. 2011, *MNRAS*, 411, 247
- Rogerson, J. A., Hall, P. B., Rodríguez Hidalgo, P., et al. 2016, *MNRAS*, 457, 405
- Rupke, D. S., Veilleux, S., & Sanders, D. B. 2002, *ApJ*, 570, 588
- Shen, Y., Richards, G. T., Strauss, M. A., et al. 2011, *ApJS*, 194, 45
- Streblyanska, A., Barcons, X., Carrera, F. J., & Gil-Merino, R. 2010, *X-ray Astronomy 2009; Present Status, Multi-Wavelength Approach and Future Perspectives*, 1248, 513
- Teng, S. H., Brandt, W. N., Harrison, F. A., et al. 2014, *ApJ*, 785, 19
- Trump, J. R., Hall, P. B., Reichard, T. A., et al. 2006, *ApJS*, 165, 1
- Vilkoviskij, E. Y., & Irwin, M. J. 2001, *MNRAS*, 321, 4
- Vivek, M., Srianand, R., & Gupta, N. 2016, *MNRAS*, 455, 136
- Vivek, M., Srianand, R., Petitjean, P., et al. 2014, *MNRAS*, 440, 799
- Weymann, R. J., Morris, S. L., Foltz, C. B., & Hewett, P. C. 1991, *ApJ*, 373, 23
- Xu, X., Arav, N., Miller, T., & Benn, C. 2018, *ArXiv e-prints*, arXiv:1805.01544